catalysts

MDPI

Article

Cobalt-Doped Hydrochar Derived from Microalgae as an Efficient Peroxymonosulfate Activator for Paraben Degradation

Chenyan Hu [1,2,†], Suxin Wu [1,†], Jiali Wang [1] and Lianguo Chen [3,*]

[1] School of Chemistry and Environmental Engineering, Wuhan Institute of Technology, Wuhan 430072, China; huchenyan1984@126.com (C.H.); suxinwu1018@163.com (S.W.); jiali_w2022@163.com (J.W.)
[2] Engineering Research Center of Phosphorus Resources Development and Utilization of Ministry of Education, Wuhan 430072, China
[3] State Key Laboratory of Freshwater Ecology and Biotechnology, Institute of Hydrobiology, Chinese Academy of Sciences, Wuhan 430072, China
* Correspondence: lchenam@ihb.ac.cn; Tel.: +86-27-68780042
† These authors contributed equally to this work.

Abstract: Hydrochar, an attractive member of the carbonaceous materials, is derived from biomass and projects great potential in peroxymonosulfate (PMS) activation, but has not been studied much. Herein, by using the large-scale cultured *Chlorella vulgaris* and field-collected bloom algae, a series of porous hydrochar was synthesized via a facile hydrothermal carbonization reaction, while Co doping significantly increased their specific surface areas, carbonization degree, and surface functional groups. These Co-doped hydrochar (xCo-HC, x: amount of the Co precursor) could efficiently activate the PMS, resulting in nearly 100% removal of five common paraben pollutants within 40 min. A dosage of 0.2Co-HC of 0.15 g/L, a PMS concentration of 0.6 g/L, and an unadjusted pH of 6.4 were verified more appropriately for paraben degradation. The coexistence of Cl^-, SO_4^{2-}, and humic acid inhibited the degradation, while HCO_3^- showed an enhancing effect. No observable change was found at the presence of NO_3^-. Quenching results illustrated that the produced $\bullet SO_4^-$ during the conversion of doped Co^{3+}/Co^{2+} acted as the dominant active species for paraben degradation, while $\bullet O_2^-$, $^1O_2$, and •OH contributed relatively less. The algae-based hydrochar potentially facilitated the electron transfer in the xCo-HC/PMS system. Overall, this study develops a new strategy for resource utilization of the abundant algae.

Keywords: algae-derived hydrochar; PMS activation; paraben degradation; Co doping

Citation: Hu, C.; Wu, S.; Wang, J.; Chen, L. Cobalt-Doped Hydrochar Derived from Microalgae as an Efficient Peroxymonosulfate Activator for Paraben Degradation. *Catalysts* **2024**, *14*, 695. https://doi.org/10.3390/catal14100695

Academic Editor: Mohammad Mozahar Hossain

Received: 21 August 2024
Revised: 25 September 2024
Accepted: 5 October 2024
Published: 6 October 2024

1. Introduction

Parabens are a series of p-hydroxybenzoic acid esters with different alkyl or aryl groups. Due to the broad antimicrobial spectrum and chemical stability, parabens have been extensively used as preservatives in packaged foods, cosmetics, pharmaceuticals, and personal care products. For example, in food and pharmaceuticals, the concentration of parabens usually ranges from several ng/g to hundreds of μg/g [1], while up to 0.4% of a single paraben or 0.8% of the paraben mixture is allowed to be added in European cosmetics [2]. The large consumption and inappropriate disposal of paraben-containing products have unavoidably released parabens into the environment, resulting in their high detection frequency and concentrations in various water bodies, such as wastewater, surface water, seawater, groundwater, and drinking water [3–5]. Even in human urine, breast milk, serum, and placenta of pregnant women, parabens were detected at relatively high concentrations [6,7]. However, accumulative toxicological studies evidenced paraben exposure-associated health risks, including hepatotoxicity [8], neurotoxicity [9,10], carcinogenicity [11], and teratogenicity [12]. More seriously, parabens are deemed as endocrine-disrupting chemicals, which can potentially interfere with the hormonal system of the organisms, and thereby cause hormone dysfunction, impaired fertility, increased risk

of breast cancer, and so on [12–14]. Considering the widespread occurrence and adverse effects of parabens, developing effective technologies to remove them from the aquatic environment has become imperative.

In recent years, peroxymonosulfate (PMS)-based advanced oxidation process (PMS-AOP) has sparked extensive research interests in eliminating the organic pollutants from waters. Depending on the produced reactive species by activating PMS, such as sulfate radical ($\bullet SO_4^-$), hydroxyl radical ($\bullet OH$), superoxide radical ($\bullet O_2^-$), and singlet oxygen ($^1O_2$), superior removal efficiency can be achieved at relatively wide pH range and complicated conditions [15]. More notably, $\bullet SO_4^-$ possesses higher redox potential (2.6–3.1 V) and a much longer life span (30–40 μs) compared to $\bullet OH$ (1.9–2.7 V, <1 μs), which renders the PMS-AOP strategy more advantageous than other AOP processes [16]. Cobalt-based catalysts show extraordinary effects in PMS activation due to the high redox potential of Co^{3+}/Co^{2+} (E = 1.82 V) [17]. However, most of them are easily aggregated or tend to leach the toxic cobalt ions into the waters, which limits their applications. In this regard, many carbonaceous materials, such as graphene, carbon nanotubes, activated carbon, and biochar, have been explored as matrices for uniformly loading the cobalt and inhibiting the leaching, assisting the PMS activation [18–20]. Among these studied carbonaceous materials, low-cost biochar, which includes hydrochar and pyrochar, is considered one of the most promising and sustainable candidates [21,22]. Pyrochar is typically obtained by thermal conversion of the biomass at 300 to 800 °C under inert gas, while hydrochar is prepared by comparatively mild hydrothermal carbonization (HTC) at 150–250 °C and self-generated pressure without drying the wet biomass beforehand [23]. Compared with its more popular sibling, pyrochar, hydrochar retains abundant oxygen-containing groups and has more merits in environmental friendliness and energy consumption. However, less attention has been paid to its utilization in PMS activation.

Due to the fast growth rates, the photoautotrophic microalgae can be easily cultured with superior CO_2 fixation capacity and no direct competition for agricultural land [24]. In terms of the algae-bloomed water bodies, harvesting and further treating the massive algae biomass is urgently needed. Meanwhile, microalgae are enriched with N, S, and P elements, which facilitates the formation of N, S, and P self-doped carbon materials without extra precursors. To date, only a few studies have focused on synthesizing microalgae-derived hydrochar, and these have only explored its application in environmental remediation by adsorption [25,26]. The potential of abundant microalgae-based hydrochar in loading transition metals as the PMS activator has barely been explored.

Herein, using large-scale cultured algae (*Chlorella vulgaris*) and field-collected bloom algae as biomass, cobalt-doped hydrochar (Co-HC) was synthesized via a facile one-step hydrothermal reaction and further employed as a PMS activator to degrade five commonly used parabens: methyl paraben (MeP), ethyl paraben (EtP), propyl paraben (PrP), butyl paraben (BuP), and benzyl paraben (BzP). Based on the activation performance of the synthesized Co-HC, the effect of hydrothermal condition, Co doping level, catalyst and PMS dosage, and the initial concentration of paraben were studied. The influence of solution pH, co-existing anions, and natural organic matter on paraben degradation was also investigated. Moreover, quenching experiments for identifying the dominant active species were carried out to unveil the mechanism. In general, this study would be helpful to explore the potential of the algae-based hydrochar in PMS activation and advance the understanding of paraben removal in the AOP process.

2. Results and Discussion

2.1. Characterization of the Catalysts

The morphologies of the synthesized pristine HC and Co-doped HC were analyzed by field emission scanning electron microscopy (FESEM). As shown in Figure 1a,b, both algae-derived carbon materials showed hierarchical porous structures. By careful observation at higher magnification (Figure 1c,d), more nanopores were found to be embodied in Co-doped HC, which could be expected to provide more active sites for catalyzing the PMS,

and also facilitate the penetration of the pollutant. Microalgae are known to accumulate elemental carbon (C) in lipids and carbohydrates, nitrogen (N) in proteins, phosphorus (P) in nucleic acids and polyphosphate pools, and sulfur (S) in sulfur-containing amino acids [24]. Here, the energy dispersive spectrometer (EDS) result illustrated that the elements of C, N, O, S, and Co were uniformly dispersed in 0.2Co-HC (Figure 1e), suggesting the successful self-doping of N, S, and exogenous doping of Co in the algae-based hydrochar. The non-observed P might be due to its low content in the algae *Chlorella vulgaris*. By using a flame atomic absorption spectrometer, the content of Co doping was measured to be 18.85 mg/g (i.e., 1.885 wt.%) in 0.2Co-HC.

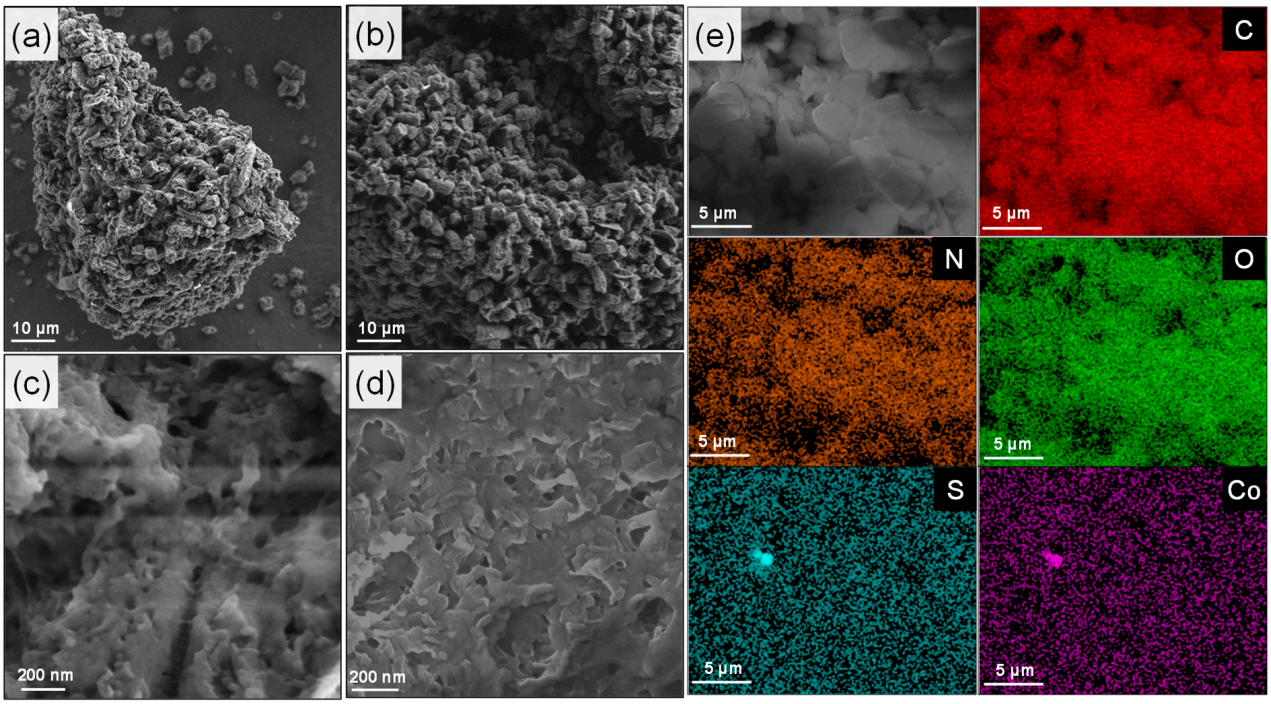

Figure 1. FESEM images of algae-derived (**a**,**c**) HC and (**b**,**d**) 0.2Co-HC under different magnifications. Both materials were synthesized at 180 °C for 12 h. (**e**) The EDS elemental mapping of 0.2Co-HC.

N_2 adsorption-desorption isotherms give more information about the porous structures of the as-prepared materials. In Figure 2a, both HC and 0.2Co-HC exhibited type IV isotherms with H3 hysteresis loops, demonstrating the existence of mesopores. During the HTC process, a series of carbonization reactions (e.g., hydrolysis, dehydration, decarboxylation, condensation, polymerization, and aromatization) occurred to the algae components in a parallel network, contributing to the generated micropores and mesopores in HC and 0.2Co-HC [27]. Based on their BJH pore size distribution (Figure S1), approximately 22 nm pores were observed in 0.2Co-HC, while HC had approximately 60 nm pores. In conjunction with the SEM analysis, it is clear that Co doping promoted the formation of more mesopores in 0.2Co-HC, consequently increasing its specific surface area to 19.14 m^2/g compared to the pristine HC (5.59 m^2/g) (inset of Figure 2a).

XRD diffraction patterns of HC and 0.2Co-HC are delineated in Figure 2b, where a broad peak centered at about 22.8° is noted for each, indicating their amorphous carbon structures [28]. The absence of a cobalt-related peak in 0.2Co-HC suggested that Co had been potentially doped into the carbon network, instead of forming any oxides on the surface. Both Raman spectra of HC and 0.2Co-HC displayed two characteristic peaks at 1360 cm^{-1} (D band) and 1580 cm^{-1} (G band) (Figure 2c), corresponding to the defect/disordered carbon and crystalline graphitic carbon, respectively. Compared to HC (I_D/I_G = 0.81), the lowered intensity ratio of 0.2Co-HC (I_D/I_G = 0.77) revealed its increased graphitization degree [29]. As a Lewis acid, the added $Co(NO_3)_2$ precursor might be capa-

ble of catalyzing the HTC process, resulting in the enhanced carbonization of the obtained material. According to an earlier study, the enhanced graphitization degree of the Co-doped hydrochar means more sp2 carbons with plentiful free-flowing π electrons existed, which could possibly improve its electronic conductivity [19,29]. In order to confirm that, the electrochemical impedance tests were performed, and a smaller arc radius was portrayed by 0.2Co-HC (Figure S2), reflecting its minimized electron transfer resistance.

The surface functional groups of the synthesized materials were scrutinized by FTIR. As displayed in Figure 2d, both the pristine HC and 0.2Co-HC had a peak at 698 cm^{-1}, representing the triazine units [23]. Meanwhile, hydroxyl groups (-OH) (3418 cm^{-1}, 1633 cm^{-1}), N-H (3284 cm^{-1}), nonpolar alkyl-CH_2 (2929 cm^{-1}, 2860 cm^{-1}), unsaturated aromatic C=C/C=O (1531 cm^{-1}, 1456 cm^{-1}), phenolic C-OH (1396 cm^{-1}), and aliphatic C-O-C (1239 cm^{-1}) were also exhibited [15,30,31], implying that hydrochar contains abundant surface function groups. It is notable to see that Co doping intensified these functional groups in 0.2Co-HC relative to the pristine HC, especially the C-OH and C-O groups, which was verified to facilitate the PMS activation [30].

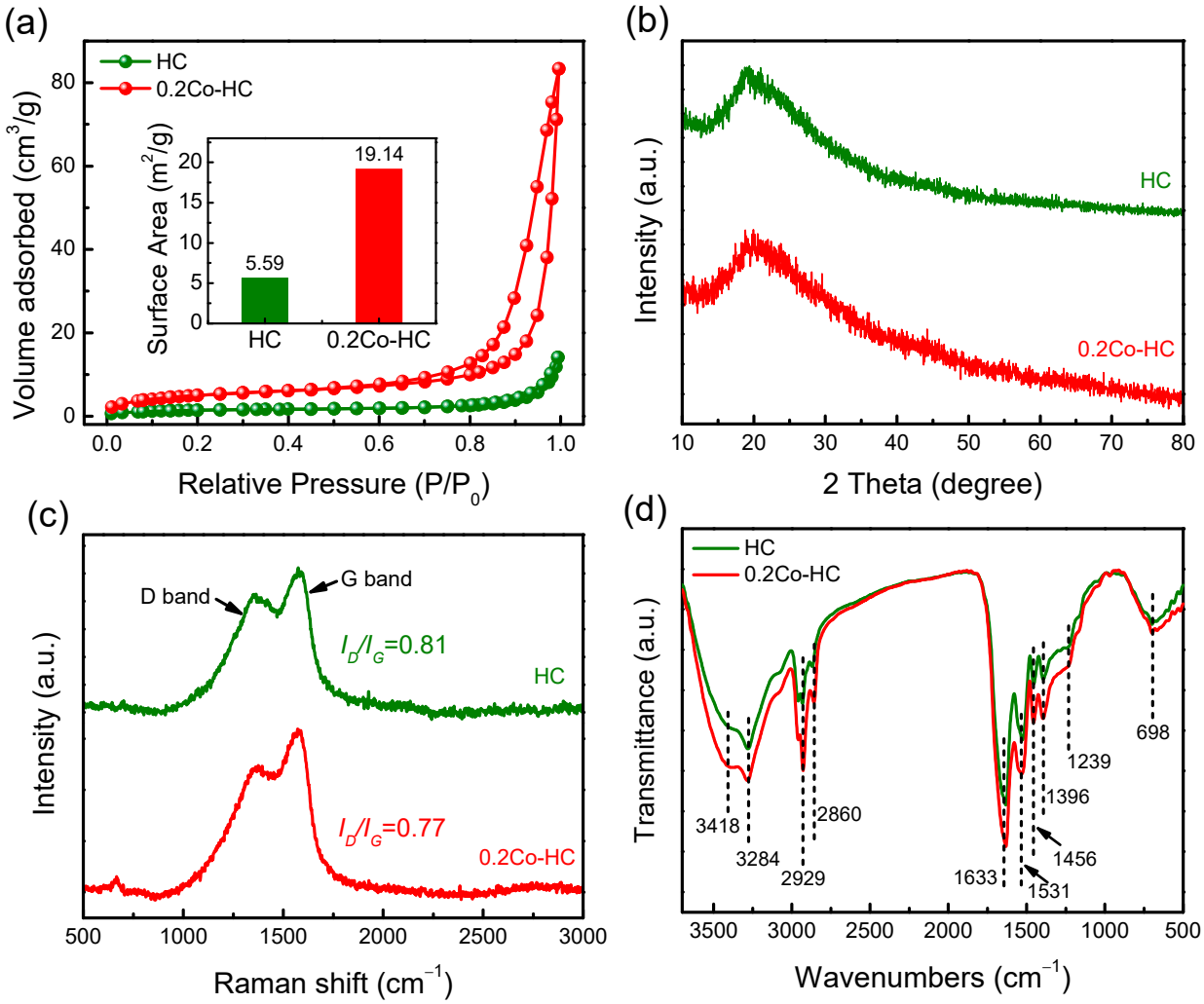

Figure 2. (**a**) N_2 adsorption–desorption isotherms of HC and 0.2Co-HC. Inset is their measured specific surface area. (**b**–**d**) is XRD diffraction patterns, Raman spectra, and FTIR spectra of HC and 0.2Co-HC, respectively.

XPS analysis was used to examine the chemical states of the hydrochar. The survey spectra disclosed the main elements in HC and 0.2Co-HC (Figure 3a), which were C, N, O, and S. Different from HC, Co only existed in 0.2Co-HC, further confirming its successful doping. The C 1s spectra of HC and 0.2Co-HC portrayed three deconvoluted peaks at

284.8 eV (C-C/CH_X/C=C), 286.0 eV (C-OH/C-N), and 288.1 eV (C=O) (Figure 3b). Their relative atomic percentages are listed in Table S1. For the N 1s spectra, the split three peaks (399.2 eV, 400.0 eV, and 400.7 eV) of both hydrochar could be ascribed into pyridinic N, pyrrolic N, and graphitic N, respectively (Figure 3c). As a result of the Co doping, a notable discrepancy occurred to their contents in pristine HC and 0.2Co-HC, showing significantly increased pyrrolic N, with decreased pyridinic N and graphitic N in 0.2Co-HC (Table S1). The O 1s profiles of the hydrochar could also be fitted into three peaks at binding energies of 531.3 eV, 532.1 eV, and 533.3 eV (Figure 3d), attributable to C=O, C-O-C/C-OH, and N−O, respectively [32,33]. Co doping was potentially conducive to the formation of C=O, leading to its increased content in 0.2Co-HC (Table S1). Both S 2p spectra of the pristine HC and 0.2Co-HC were decomposed into C–S at 163.6 eV and C-SO_x at 167.5 eV (Figure 3e) [34]. Figure 3f shows the Co 2p spectrum of 0.2Co-HC. The deconvoluted peaks at 780.4 eV and 795.9 eV were assigned to Co^{3+} 2p3/2 and 2p1/2, while the peaks at 781.6 eV and 797.2 eV were associated with Co^{2+} 2p3/2 and 2p1/2, respectively. As can be seen, the doped Co existed in the form of Co^{3+} and Co^{2+} in the hydrochar. The other two peaks at 785.3 eV and 801.8 eV belonged to the associated shake-up satellite peaks of Co^{2+} 2p3/2 and Co^{2+} 2p1/2 [35].

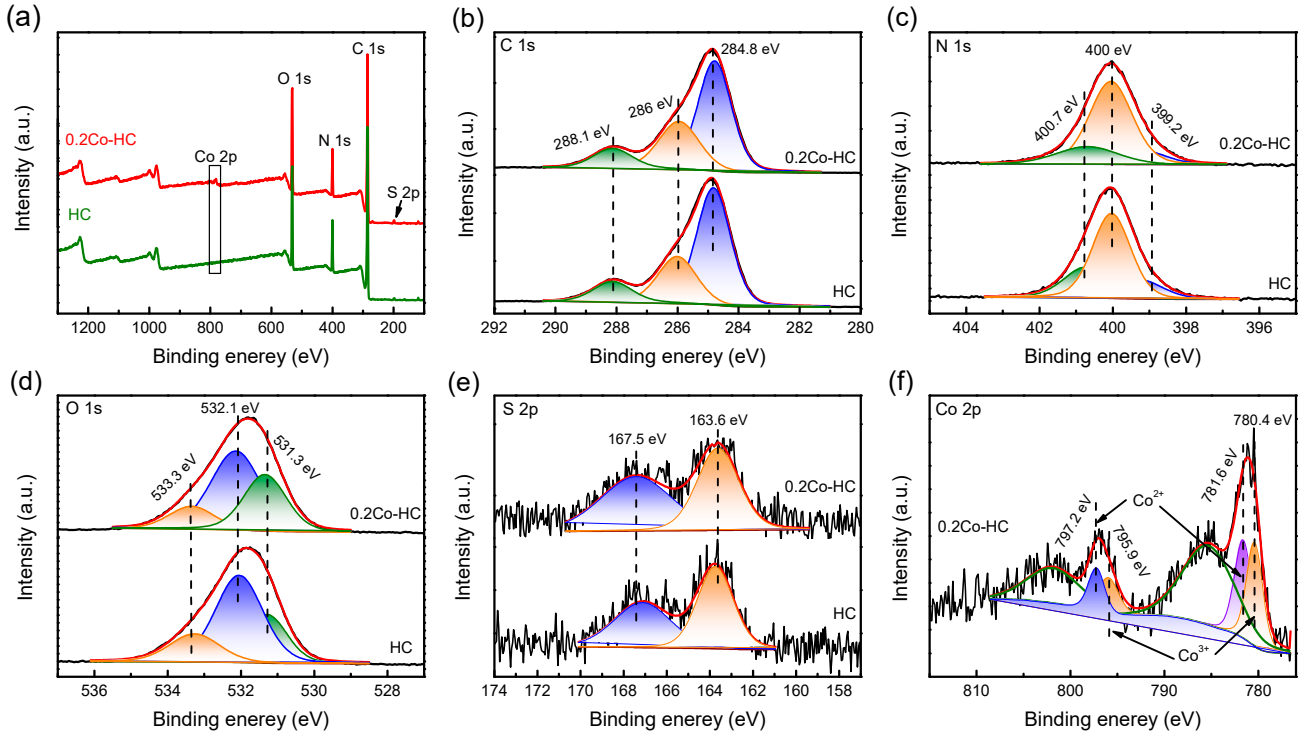

Figure 3. XPS (**a**) survey, (**b**) C 1s, (**c**) N 1s, (**d**) O 1s, and (**e**) S 2p spectra of HC and 0.2Co-HC. (**f**) Co 2p spectrum of 0.2Co-HC.

2.2. Paraben Degradation in Activated PMS System by Co-Doped Hydrochar

The PMS activation performances of the algae-derived hydrochar were initially assessed by removing MeP, the most detected paraben preservative in the environment. Differently sourced algae (massively cultured *Chlorella vulgaris* and field-collected bloom algae) were used as the feedstock for the hydrochar preparation. As shown in Figure 4a, about 8% of MeP was adsorbed on *Chlorella vulgaris*-derived HC, and no further degradation by activated PMS could be observed. In contrast, Co-doped HC remarkably promoted the MeP removal, achieving the efficiency of 98.7%, 68%, and 31%, respectively, by 0.4Co-HC, 0.2Co-HC, and 0.1Co-HC within 20 min. When extending the reaction to 40 min, 0.2Co-HC/PMS could also degrade 98.2% of MeP. Towards MeP, all these Co-doped HC exhibited similar adsorption capacities (~7%) to that of the pristine one, inferring that the

Co doping primarily boosted the catalytic performance for PMS activation, rather than enhancing the MeP adsorption. With increasing the Co doping amount, the first order kinetic constant (*K*) of 0.1Co-HC, 0.2Co-HC, and 0.4Co-HC rose from 0.0186 min^{-1} and 0.0648 min^{-1} to 0.1304 min^{-1}, indicating the great contribution of Co doping to PMS catalysis (Figure 4b). The influences of the hydrothermal temperature and duration were studied in Figure S3, witnessing the proper HTC condition at 180 °C for 12 h.

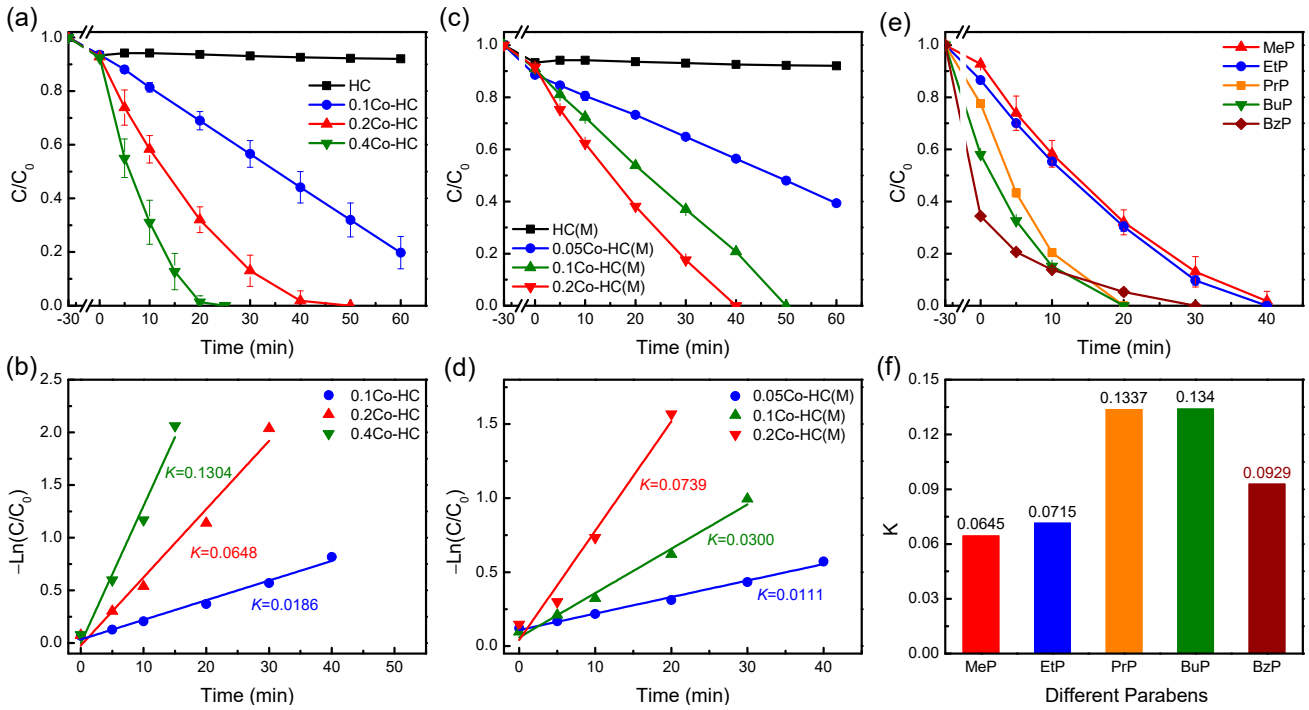

Figure 4. Degradation of MeP in activated PMS systems by (**a**) massively cultured algae *Chlorella vulgaris* and (**c**) field-collected bloom algae-derived HC and Co-doped HC with different Co contents. (**b**,**d**) are the corresponding first-order kinetics of (**a**,**c**). (**e**) Degradation of different parabens by 0.2Co-HC/PMS and (**f**) its first-order kinetics. ([0.2Co-HC] = 0.15 g/L, [MeP] = 10 mg/L, [PMS] = 0.6 g/L, HC and Co-HC were synthesized at 180 °C for 12 h).

When using the field-collected bloom algae to synthesize the hydrochar, the Co-doped HC(M)/PMS system was also capable of removing MeP with desired performance (Figure 4c,d), showing the good applicability of this resource utilization of algae biomass. Similarly, enhanced degradation efficiency and rate were attained by increasing the Co doping amount. Although 0.057 mg/L Co (~2%) was detected to gradually leach out (Figure S4a) in the 0.2Co-HC/PMS system, the equal amount of Co^{2+} as the homogeneous catalyst could only degrade 16.5% of MeP (Figure S4b), ruling out the potential effect from the dissolved Co. Therefore, the efficient activation of PMS should be mainly attributed to the doped Co^{2+} and Co^{3+}, whose redox cycles might initiate the PMS decomposition, and thereby generate the active species for paraben degradation. During these processes, the Co-doped hydrochar supporter with increased pore numbers, enhanced surface area, and improved electronic conductivity would be significantly involved by facilitating the penetration of paraben pollutants, providing more reaction sites, and accelerating the electron transfer [17]. In the case of the potential Co leaching in higher doped material, 0.2Co-HC was used for the following investigation.

With regard to other paraben preservatives (EtP, PrP, BuP, and BzP), 0.2Co-HC activated PMS system also showed extraordinary removal performance (Figure 4e). Specifically, nearly 100% of EtP was eliminated in 40 min, while the removal of PrP and BuP only needed 20 min. It is worth noting that the adsorption of these parabens on 0.2Co-HC was essentially influenced by their structures, revealing the increased adsorption with more complicated

side chains for the following: BzP (65.6%) > BuP (42.0%) > PrP (22.5%) > EtP (13.4%) > MeP (7.2%). This trend was consistent with their adsorption on other graphene-family nanomaterials (i.e., graphene oxide, multilayered graphene, graphene oxide), and believed to be dominated by hydrophobic interaction [36]. The strong adsorption of the paraben on 0.2Co-HC favored its degradation in the activated PMS system, eliciting the increased degradation rate (*K*) from MeP (0.0645 min^{-1}) to BuP (0.134 min^{-1}) (Figure 4f). The excess adsorption of BzP might cover the reaction sites, which thereby induced the decreased degradation rate (0.0929 min^{-1}) relative to BuP.

2.3. Effects of Different Parameters on MeP Degradation in Co-HC/PMS System

Impacts of the catalyst and PMS dosage, MeP concentration, and the initial solution pH on MeP degradation in 0.2Co-HC/PMS system were explored since they had the potential to dramatically influence the catalytic performance. When the dosage of 0.2Co-HC increased from 0.05 g/L to 0.15 g/L, the removal efficiency of MeP in 40 min was enhanced from 59.8% to 98.2% (Figure 5a), while the corresponding *K* was augmented from 0.0196 min^{-1} to 0.0648 min^{-1} (Figure S5a). Higher catalyst dosage provided more active sites for PMS activation, leading to more efficient MeP degradation [37]. Beyond 0.15 g/L, the active sites were not the limiting step anymore, manifesting the unchanged activity of 0.3 g/L to 0.15 g/L. The effect of PMS dosage is depicted in Figure 5b and Figure S5b. An improved degradation performance was observed when PMS concentration increased from 0.4 g/L to 0.5 g/L. Although further increasing the PMS dosage to 0.6 g/L and 0.7 g/L would yield more active species, the self-quenching and active site competition between excess PMS and MeP resulted in their similar effects to the 0.5 g/L [37]. As the concentration of MeP increased from 5 mg/L to 30 mg/L, the removal performance of MeP declined prominently (Figure 5c), and the degradation rate (*K*) reduced nearly 10 times (Figure S5c). This should be explained by the relatively insufficient active species and probably blocked reaction sites at high concentrations of MeP [15].

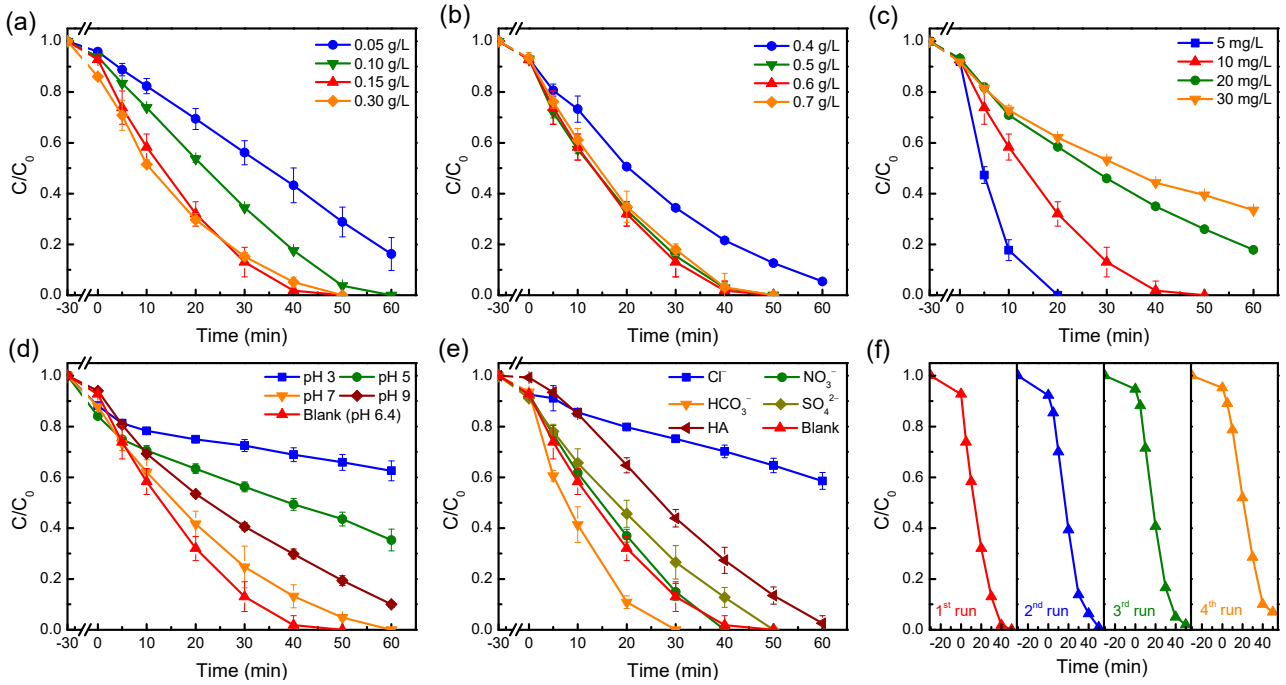

Figure 5. Impact of (**a**) catalyst dosage, (**b**) PMS dosage, (**c**) MeP concentration, (**d**) initial solution pH, and (**e**) coexisting anions and HA to MeP degradation by 0.2Co-HC/PMS. (**f**) Four consecutive experiments by reusing 0.2Co-HC. The general experimental conditions: [PMS] = 0.60 g/L, [0.2Co-HC] = 0.15 g/L, [MeP] = 10 mg/L.

The initial solution pH is another crucial parameter for the catalytic efficiency of the PMS system. As shown in Figure 5d, when pH changed from 3 to the unadjusted 6.4, MeP degradation efficiency (within 40 min) in the 0.2Co-HC/PMS system was elevated from 31.1% to 98.2%. With further increasing of the pH to 9, the efficiency gradually decreased to 70.2%. The comparison of their degradation rates (*K*) pictured the trend more clearly (Figure S5d). Here, the best degradation of MeP was observed at an unadjusted pH of 6.4, in agreement with previous work about the highest EtP degradation at a neutral pH of 6.5 using the UV/PMS process [38]. Under acidic conditions (pH 3 and 5), the unfavorable degradation may be attributed to the scavenging of $\bullet SO_4^-$ and •OH by H^+ (Equations (1) and (2)) [39]. On the other hand, raising the pH above ~8.5–9 could cause a transition from $\bullet SO_4^-$-dominated to •OH-dominated oxidation process, which possibly gave rise to the lowered degradation performance at pH 9 [40]. Meanwhile, the point of zero charge (Pzc) of 0.2Co-HC was evaluated to bed 4.43 (Figure S6). The *p*Ka value of MeP was reported to be 8.31 [41]. In this way, both 0.2Co-HC and MeP would be negatively charged at pH 9. The as-formed electrostatic repulsion between 0.2Co-HC, MeP, and PMS (HSO_5^- and SO_5^{2-}) was also adverse to MeP degradation.

$$\bullet SO_4^- + H^+ + e^- \rightarrow HSO_4^- \quad (1)$$

$$\bullet OH + H^+ + e^- \rightarrow H_2O \quad (2)$$

In natural water bodies, various anions and organic matter exist. To probe their effects on paraben degradation by 0.2Co-HC/PMS, the common anions (Cl^-, NO_3^-, HCO_3^-, and SO_4^{2-}) and humic acid (HA) were selected as the representatives (Figures 5e and S5e). When 10 mM of Cl^- was added in the reaction process, only 41.3% of MeP could be removed even in 60 min, along with a much slower degradation rate (0.0071 min^{-1}). The markedly hindered MeP degradation might be due to the reaction of Cl^- with $\bullet SO_4^-$ and •OH to generate the less reactive chlorine-containing species (•Cl, $\bullet Cl_2^-$, and $\bullet ClHO^-$) (Equations (3)–(5)).

$$Cl^- + \bullet SO_4^- \rightarrow \bullet Cl + SO_4^{2-} \quad (3)$$

$$\bullet Cl + Cl^- \rightarrow \bullet Cl_2^- \quad (4)$$

$$Cl^- + \bullet OH \rightarrow \bullet ClHO^- \quad (5)$$

The coexistence of SO_4^{2-} had an insignificant effect on the final degradation efficiency of MeP, but mildly reduced its degradation rate (Figure S5e). Compared to marginally affected MeP degradation by NO_3^-, HCO_3^- speeded up its degradation noticeably. Although HCO_3^- may trap certain radicals (e.g., $\bullet SO_4^-$ and •OH) (Equations (6)–(8)), the formed $\bullet CO_3^-$ was very selective and preferentially abate the electron-rich organics (e.g., MeP) [16]. HCO_3^- was also reported to directly activate the PMS and produce $^1O_2$. These two factors may contribute to the accelerated MeP degradation.

$$HCO_3^- + \bullet OH \rightarrow H_2O + \bullet CO_3^- \quad (6)$$

$$HCO_3^- + \bullet SO_4^- \rightarrow SO_4^{2-} + \bullet CO_3^- + H^+ \quad (7)$$

$$HCO_3^- + HSO_5^- \rightarrow SO_4^{2-} + HCO_4^- + H^+ \quad (8)$$

As one of the most typical natural organic matters, HA retarded the degradation of MeP from 0.0648 min^{-1} to 0.0323 min^{-1}. When coexisting with HA, the hardly adsorbed MeP (<1%) implied that HA might occupy the 0.2Co-HC surface via strong π-π stacking, which obstructed the interaction of 0.2Co-HC, PMS, and MeP. Additionally, HA would compete with MeP for the reactive species (e.g., $\bullet SO_4^-$ and •OH), thereby reducing its removal rate [42].

The reusability and stability properties of 0.2Co-HC were demonstrated in Figure 5f. During the four consecutive tests, the reused activator 0.2Co-HC kept an acceptable degra-

dation efficiency of MeP (>92%), but the degradation rate gradually decreased (Figure S5f), which might be due to the saturated adsorption of 0.2Co-HC and leaching of cobalt.

2.4. Possible Mechanism for Co-HC Activated PMS System

Quenching experiments were conducted to distinguish the contribution of different active species to MeP degradation in a 0.2Co-HC-activated PMS system. Methanol (MeOH) was applied to quench both •OH and $•SO_4^-$ ($K_{•SO4^-/MeOH}$ = 1.1 × 10^7 M^{-1} s^{-1}, $K_{•OH/MeOH}$ = 9.7 × 10^8 M^{-1} s^{-1}), while tert-butanol (TBA) was targeted on •OH ($K_{•SO4^-/TBA}$ = (4–9.1) × 10^5 M^{-1} s^{-1}, $K_{•OH/TBA}$ = (3.8–7.6) × 10^8 M^{-1} s^{-1}) [43]. Benzoquinone (BQ) and L-histidine (L-his) were employed as the quenching agents for the corresponding $•O_2^-$ (K = 1.0 × 10^9 M^{-1} s^{-1}) and $^1O_2$ (K =3.2 × 10^7 M^{-1} s^{-1}) [17]. As illustrated in Figure 6a, the addition of MeOH (0.1 and 0.2 M) dramatically suppressed the MeP elimination, but TBA had limited impacts. These results suggested that the produced $•SO_4^-$ by 0.2Co-HC-activated PMS may work as the main reactive species for MeP degradation, while •OH played a minor role. The specific signals of •OH and $•SO_4^-$ detected in the electron paramagnetic resonance (EPR) spectrum of the 0.2Co-HC/PMS system further identified their generation (Figure 6b). When 1 and 5 mM of BQ was added, the degradation of MeP was inhibited to only ~67% in 60 min, and L-his brought about the gradually decreased MeP degradation. Figure 6c,d verified the production of $•O_2^-$ and $^1O_2$, so it is reasonable to conclude that they could participate in the degradation process, but contribute relatively less than $•SO_4^-$. The signals of TMPO-$^1O_2$ adduct were notably intensified with the increased duration, reflecting the accumulation of $^1O_2$. In contrast to that, the EPR signals of $•O_2^-$ did not show an obvious change with time, possibly due to its fast conversion to $^1O_2$ (Equations (9)).

$$2•O_2^- + 2H_2O \rightarrow {}^1O_2 + H_2O_2 + 2HO^- \quad (9)$$

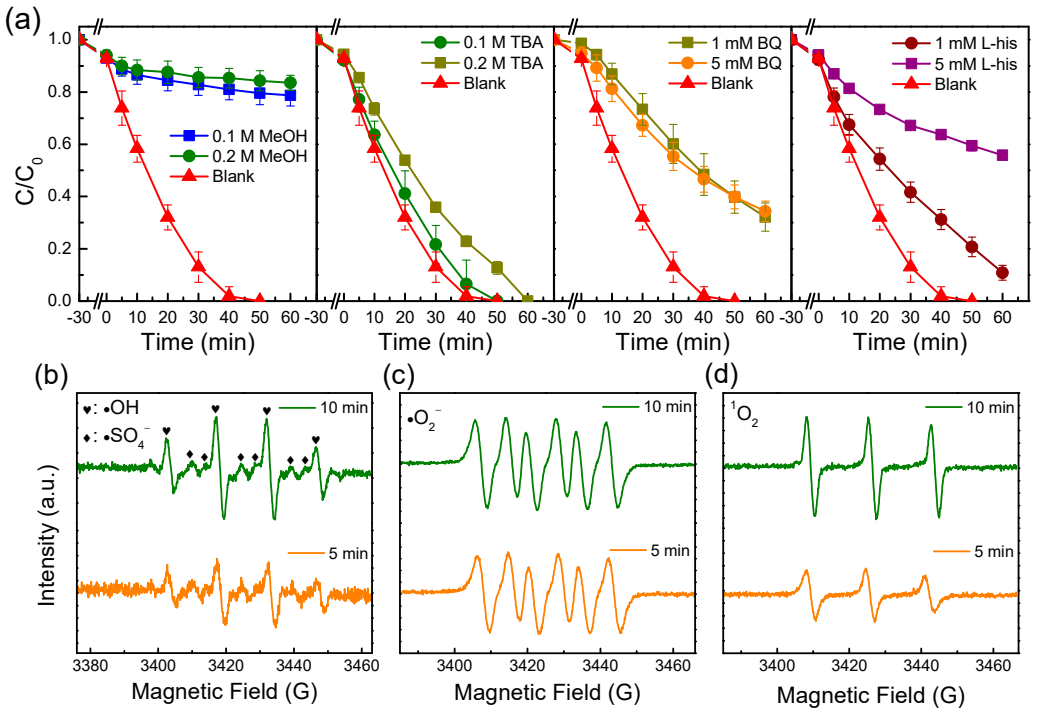

Figure 6. (**a**) The effects of MeOH, TBA, BQ, and L-his on MeP degradation in 0.2Co-HC/PMS system. ([0.2Co-HC] = 0.15 g/L, [PMS] = 0.6 g/L, [PMS] = 10 mg/L). (**b**) DMPO—•OH and DMPO—$•SO_4^-$, (**c**) DMPO—$•O_2^-$, and (**d**) TMPO-$^1O_2$ EPR spin trapping spectra of 0.2Co-HC/PMS system.

In order to investigate the origin of these active species, XPS analysis was carried out on the used 0.2Co-HC material. Compared to the fresh sample (Figure 3), the Co 2p and N 1s spectra of the reacted 0.2Co-HC showed an observable difference (Figure 7, Table S1), emphasizing their active involvement in the reaction. Notably, the proportion of Co^{3+} increased and Co^{2+} conversely decreased, indicating a potential redox cycle between Co^{3+} and Co^{2+}. Meanwhile, the content of the pyrrolic N significantly decreased from 67.4% to 43.7% after the reaction, pointing out its possible function as the Co binding sites [29].

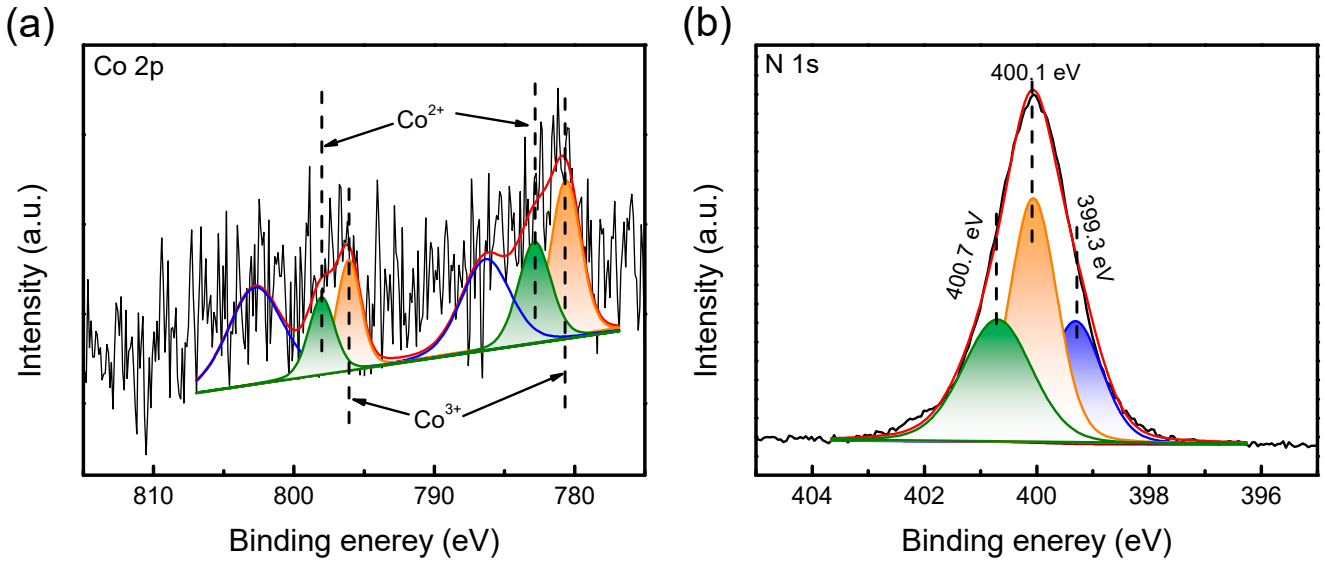

Figure 7. High-resolution (**a**) Co 2p and (**b**) N 1s XPS spectra of used 0.2Co-HC.

Based on the above results, the underlying mechanism for PMS activation by Co-doped hydrochar was proposed in Figure 8. During the HTC process, Co ions may be mobilized in the formed hydrochar by coordinating with pyrrolic N sites. Since the redox potential of Co^{3+}/Co^{2+} (E = 1.82 V) is higher than that of $HSO_5^-/\bullet SO_5^-$ (E = 1.10 V), the doped Co^{2+} will react with HSO_5^- to produce $\bullet SO_4^-$ and •OH (Equations (10) and (11)). Meanwhile, Co^{3+} will be reduced to Co^{2+} by PMS with the resultant formation of $\bullet SO_5^-$ (Equation (12)). Considering the enhanced carbonization degree and surface function groups, the Co-doped hydrochar could not only facilitate the electron transfer but also promote the formation of $\bullet O_2^-$ and $^1O_2$ via Equations (9) and (13)–(15). Depending on these generated active species ($\bullet SO_4^-$, $\bullet SO_5^-$, •OH, $\bullet O_2^-$, $^1O_2$, etc.), the Co^{2+}- and Co^{3+}-doped hydrochar maintained the high utilization of PMS and effectively degraded the paraben preservatives.

$$Co^{2+} + HSO_5^- \rightarrow Co^{3+} + \bullet SO_4^- + OH^- \quad (10)$$

$$\bullet SO_4^- + H_2O \rightarrow H^+ + SO_4^{2-} + \bullet OH \quad (11)$$

$$Co^{3+} + HSO_5^- \rightarrow Co^{2+} + \bullet SO_5^- + H^+ \quad (12)$$

$$Co\text{-}HC + O_2 \rightarrow \bullet O_2^- + Co\text{-}HC^+ \quad (13)$$

$$\bullet OH + H_2O_2 \rightarrow \bullet HO_2 + H_2O \quad (14)$$

$$\bullet HO_2 \rightarrow \bullet O_2^- + H^+ \quad (15)$$

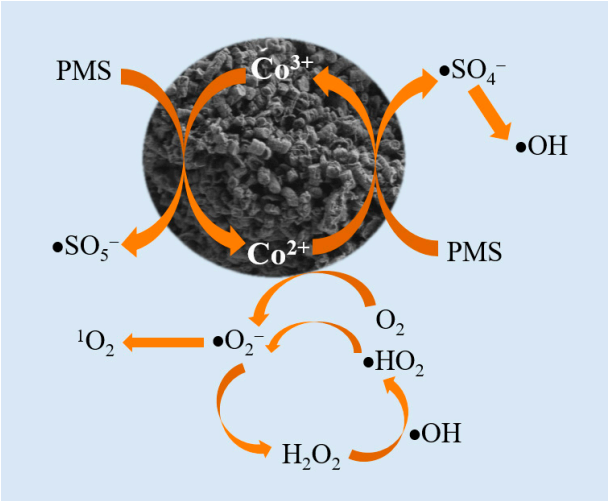

Figure 8. Proposed mechanism of PMS activation by Co-doped hydrochar.

3. Materials and Methods

3.1. Reagents and Chemicals

Potassium peroxymonosulfate (PMS, $KHSO_5 \geq 42.8\%$), p-benzoquinone (BQ), L-Histidine (L-His), and Nafion (5 wt.%) were purchased from Aldrich (Shanghai, China). Cobalt nitrate hexahydrate ($Co(NO_3)_2 \cdot 6H_2O$, 99.99%), propyl paraben, and butyl paraben were purchased from Macklin Chemical Technology Co., Ltd., (Shanghai, China). Methyl paraben, ethyl paraben, benzyl paraben, sodium chloride, sodium sulfate, sodium bicarbonate, sodium nitrate, methanol (MeOH), tert-butanol (TBA), and nitric acid were bought from Sinopharm Chemical Reagent Co., Ltd. (Shanghai, China). Humic acid was obtained from Tianjin Guangfu Fine Chemical Research Institute. In order to check the applicability of the method, the massively cultured *Chlorella vulgaris* and field-collected bloom algae were chosen as the precursors for hydrochar synthesis. *Chlorella vulgaris* powder was attained from Shenzhen Yide Biotechnology Co., Ltd. (Shenzhen, China). The bloom algae were collected from a wild pond in Wuhan, China, and the dominant species was identified to be *Microcystis* sp (93.32%). The properties and pre-treatment method of the collected algae could be referred to in our earlier report [34]. Ultrapure water (18.25 MΩ cm^{-1}) was used in this work.

3.2. Synthesis of the Catalysts

The hydrothermal reaction was carried out in a Teflon-lined autoclave. Before the reaction, the algae powder was pre-treated with a nitric acid solution to break the cell well. Typically, 2 g of the algae powder (*Chlorella vulgaris*) was immersed in 100 mL of nitric acid solution (4 M) under continuous ultrasonication for 1 h, and then washed with water by centrifugation until the pH became neutral. The obtained precipitate was added with 40 mL water, along with a certain amount of $Co(NO_3)_2 \cdot 6H_2O$ (0.1 g, 0.2 g, and 0.4 g). After being stirred for 30 min, the mixture was transferred to the autoclave for a hydrothermal carbonization reaction. The hydrothermal temperature varied at 160, 180 °C, and 200 °C, respectively. The duration lasted for 6, 12, and 18 h, individually. Without specific indication, the materials were synthesized at 180 °C for 12 h. When cooling down to room temperature, the obtained powder was collected by centrifugation at 10,000 rpm for 15 min, washed with water and ethanol, and then dried at 60 °C overnight. According to the added amount of $Co(NO_3)_2 \cdot 6H_2O$, the synthesized products were named 0.1Co-HC, 0.2Co-HC, and 0.4Co-HC. Meanwhile, the hydrochar prepared via the same method but without $Co(NO_3)_2 \cdot 6H_2O$ was labeled as HC. For comparison, the same procedure was also applied to the field-collected algae, and the obtained samples were referred to as HC(M), 0.1Co-HC(M), 0.2Co-HC(M), and 0.4Co-HC(M), respectively.

3.3. Characterization

The morphologies of the synthesized materials were examined by field emission-scanning electron microscopy (FESEM) (ZEISS GeminiSEM 300, Jena, Germany). The crystal structures of the materials were investigated by X-ray diffraction (XRD) (Bruker, Karlsruhe, Germany) at a scan rate of 5°/min. X-ray photoelectron spectroscopy (XPS) analysis was performed by ThermoFischer ESCALAB 250Xi (Thermo Fisher, Waltham, MA, USA). Fourier transform infrared (FTIR) spectra were recorded by a KBr pallet technique using a Nicolet-6700 spectrometer (Thermo Electron, Waltham, MA, USA). Raman spectra were monitored on a DXR Raman spectrometer equipped with an Ar laser at 532 nm (Thermo Fisher, Waltham, MA, USA). A Brunauer–Emmett–Teller (BET) measurement was performed on ASAP2020 HD88 (Micromeritics, Norcross, GA, USA), Micromeritics. The leaching amount of Co ions in the filtered reaction solution was directly quantified by a flame atomic absorption spectrometer (SP-3520AA, Shanghai, China). When identifying the doped Co content, the synthesized hydrochar samples were digested by the fresh aqua regia at 120 °C for 8 h, and then measured by the flame atomic absorption spectrometer.

3.4. Catalytic Performance

PMS activation abilities of the prepared hydrochar materials were evaluated by paraben degradation. Initially, a certain amount of the catalyst (0.005–0.03 g) was added into 100 mL of paraben solution (10 mg/L), which was stirred for 30 min to reach the adsorption-desorption equilibrium. H_2SO_4 or NaOH solution (0.1 M) was used for pH adjustment when necessary. Then, PMS (0.4–0.7 g/L) was added to the mixture to launch the degradation. At a certain time interval, 4 mL of the reaction solution was taken, quenched by 0.5 mL of methanol immediately, and then filtered through a 0.22 μm PTFE membrane. The concentrations of the paraben residual were quantified using an Agilent 1260 high-performance liquid chromatograph (HPLC) equipped with a C18 reversed-phase column (Zorbax SB-Aq, Agilent, Santa Clara, CA, USA) and a diode array detector (DAD). The injection volume was 20 μL, and the mobile phase was a mixture of methanol and water (60:40, *v*/*v*) at a flow rate of 0.8 mL/min. The detection wavelength was 256 nm. The degradation efficiency was calculated by $(1 - C/C_0) \times 100\%$, where C_0 and C are the initial and residual concentrations of the treated paraben, respectively. The pseudo-first-order kinetic model was described as $\mathrm{Ln}(C/C_0) = -Kt$, where K is the pseudo-first-order kinetic constant (K). All experiments were executed at least three times to eliminate the experimental errors.

Different reaction conditions, such as catalyst and PMS dosages, pH value, the initial concentration of paraben, as well as the different paraben species, were investigated. The effects of co-existing anions on paraben degradation were studied in the presence of 10 mM NaCl, $NaNO_3$, $NaHCO_3$, and Na_2SO_4, respectively. Humic acid (10 mg/L) was used as the representative of natural organic matter to check its influence on paraben removal. Quenching experiments were conducted by using MeOH, TBA, BQ, and L-His as quenching agents for different reactive oxidation species. Electron paramagnetic resonance (EPR) spectra were recorded on an EMXnano spectrometer (Bruker, Karlsruhe, Germany) by using DMPO and TEMP as the spin trappers. For the recycling experiment, the used catalysts were collected, washed with water and ethanol, dried at 60 °C, and then reused for the next run.

4. Conclusions

In summary, the Co-doped hydrochar was prepared by using the massively cultured pure algae as well as naturally collected bloom algae as the precursors, which demonstrated the good applicability of this facile strategy. During the HTC process, the Co doping also facilitated the synthesized hydrochar supporter with increased pore numbers, enhanced surface area, and functional groups, and improved electronic conductivity. When employed as the PMS activator, these Co-doped hydrochars exhibited favorable activity in eliminating the paraben pollutants, which was mainly ascribed to the doped Co^{2+} and Co^{3+}. During the conversion process of Co^{2+}/Co^{3+}, PMS was decomposed to generate the active $\bullet SO_4^-$ for

paraben degradation. $\bullet O_2^-$, $^1O_2$, and •OH were also produced, but contributed relatively less. This study provides a new measure and utilization of the abundant and renewable algae biomass, which also helps the treatment of organic pollutants in waters.

Supplementary Materials: The following supporting information can be downloaded at the following link: https://www.mdpi.com/article/10.3390/catal14100695/s1, Figure S1. BJH pore size distribution of the synthesized HC and 0.2Co-HC. Figure S2. EIS Nyquist plots of HC and 0.2Co-HC. Figure S3. The influence of hydrothermal (b) temperature and (c) duration on the catalytic performance of 0.2Co-HC/PMS. Figure S4. (a) The leached Co ions during the MeP degradation process by 0.2Co-HC/PMS. (b) The degradation of MeP by 0.057 mg/L Co^{2+} and 0.2Co-HC activated PMS. ([0.2Co-HC] = 0.15 g/L, [MeP] = 10 mg/L, [PMS] = 0.6 g/L). Figure S5. The first order kinetics or the constant *K* of (a) PMS dosage, (b) catalyst dosage, (c) MeP concentration, (d) initial solution pH, and (e) coexisting anions and HA influenced MeP degradation by 0.2Co-HC/PMS. (f) The first-order kinetic constant *K* of four consecutive experiments by reusing 0.2Co-HC. The general experimental conditions: [PMS] = 0.6 g/L, [0.2Co-HC] = 0.15 g/L, [MeP] = 10 mg/L. Figure S6. P_{ZC} of 0.2Co-HC. Figure S7. High-resolution (a) C 1s and (b) O 1s XPS spectra of used 0.2Co-HC after PMS activation; Table S1. Atomic percentages of elements in different hydrochar.

Author Contributions: Conceptualization, C.H.; Methodology, S.W. and J.W.; Project administration, L.C.; Supervision, L.C.; Writing—original draft, C.H.; Writing—review and editing, L.C. All authors have read and agreed to the published version of the manuscript.

Funding: This research was funded by the National Natural Science Foundation of China (grant number 31971236), Graduate Innovative Fund of Wuhan Institute of Technology (grant number CX2023119), The Open Project of Engineering Research Center of Phosphorus Resources Development and Utilization of Ministry of Education (grant number LKF202204), The Funding for Scientific Research Projects from Wuhan Municipal Health Commission (grant number WY22A03).

Data Availability Statement: The data presented in this study are available on request from the corresponding author (L.C.).

Conflicts of Interest: The authors declare no conflicts of interest.

References

1. van der Schyff, V.; Suchankova, L.; Kademoglou, K.; Melymuk, L.; Klanova, J. Parabens and antimicrobial compounds in conventional and "green" personal care products. *Chemosphere* **2022**, *297*, 134019. [CrossRef] [PubMed]
2. Wei, F.; Mortimer, M.; Cheng, H.; Sang, N.; Guo, L.-H. Parabens as chemicals of emerging concern in the environment and humans: A review. *Sci. Total Environ.* **2021**, *778*, 146150. [CrossRef] [PubMed]
3. Pereira, A.R.; Simoes, M.; Gomes, I.B. Parabens as environmental contaminants of aquatic systems affecting water quality and microbial dynamics. *Sci. Total Environ.* **2023**, *905*, 167332. [CrossRef]
4. K'oreje, K.; Okoth, M.; Van Langenhove, H.; Demeestere, K. Occurrence and point-of-use treatment of contaminants of emerging concern in groundwater of the Nzoia River basin, Kenya. *Environ. Pollut.* **2022**, *297*, 118725. [CrossRef] [PubMed]
5. Lu, S.; Wang, N.; Ma, S.; Hu, X.; Kang, L.; Yu, Y. Parabens and triclosan in shellfish from Shenzhen coastal waters: Bioindication of pollution and human health risks. *Environ. Pollut.* **2019**, *246*, 257–263. [CrossRef]
6. Assens, M.; Frederiksen, H.; Petersen, J.; Larsen, T.; Skakkebæk, N.; Juul, A.; Andersson, A.-M.; Main, K. Variations in repeated serum concentrations of UV filters, phthalates, phenols and parabens during pregnancy. *Environ. Int.* **2019**, *123*, 318–324. [CrossRef]
7. Liu, W.; Zhou, Y.; Li, J.; Sun, X.; Liu, H.; Jiang, Y.; Peng, Y.; Zhao, H.; Xia, W.; Li, Y.; et al. Parabens exposure in early pregnancy and gestational diabetes mellitus. *Environ. Int.* **2019**, *126*, 468–475. [CrossRef]
8. Hu, C.; Sun, B.; Tang, L.; Liu, M.; Huang, Z.; Zhou, X.; Chen, L. Hepatotoxicity caused by methylparaben in adult zebrafish. *Aquat. Toxicol.* **2022**, *250*, 106255. [CrossRef]
9. Hu, C.; Bai, Y.; Sun, B.; Zhou, X.; Chen, L. Exposure to methylparaben at environmentally realistic concentrations significantly impairs neuronal health in adult zebrafish. *J. Environ. Sci.* **2023**, *132*, 134–144. [CrossRef]
10. Tran, C.M.; Ra, J.-S.; Rhyu, D.Y.; Kim, K.T. Transcriptome analysis reveals differences in developmental neurotoxicity mechanism of methyl-, ethyl-, and propyl- parabens in zebrafish embryos. *Ecotox. Environ. Saf.* **2023**, *268*, 115704. [CrossRef]
11. Wu, N.; Deng, L.; Xiong, F.; Xie, J.; Li, X.; Zeng, Q.; Sun, J.; Chen, D.; Yang, P. Risk of thyroid cancer and benign nodules associated with exposure to parabens among Chinese adults in Wuhan, China. *Environ. Sci. Pollut. R.* **2022**, *29*, 70125–70134. [CrossRef]
12. Atli, E. The effects of ethylparaben and propylparaben on the development and fecundity of *Drosophila melanogaster*. *Environ. Toxicol. Pharmacol.* **2022**, *92*, 103856. [CrossRef]

13. Yan, W.; Li, M.; Guo, Q.; Li, X.; Zhou, S.; Dai, J.; Zhang, J.; Wu, M.; Tang, W.; Wen, J.; et al. Chronic exposure to propylparaben at the humanly relevant dose triggers ovarian aging in adult mice. *Ecotox. Environ. Saf.* **2022**, *235*, 113432. [CrossRef]
14. Hu, C.; Bai, Y.; Li, J.; Sun, B.; Chen, L. Endocrine disruption and reproductive impairment of methylparaben in adult zebrafish. *Food Chem. Toxicol.* **2023**, *171*, 113545. [CrossRef] [PubMed]
15. Chen, H.; Li, X.; Li, W.; Feng, J.; Zhao, Y.; Zhang, H.; Ren, Y. Nitrogen-doped biochar/MnO_2 as an efficient PMS activator for synergistic BPA degradation via non-free radical pathways in the water. *J. Environ. Chem. Eng.* **2024**, *12*, 112446. [CrossRef]
16. Lee, J.; von Gunten, U.; Kim, J.-H. Persulfate-based advanced oxidation: Critical assessment of opportunities and roadblocks. *Environ. Sci. Technol.* **2020**, *54*, 3064–3081. [CrossRef] [PubMed]
17. Zhang, J.; Xie, J.-F.; Yang, J.-C.E.; Li, D.; Zhong, L.-B.; Zheng, Y.-M. Ultra-fast degradation of ciprofloxacin by the peroxymonosulfate activation using a Co/Al-LDH decorated magnetic hydrochar: Structural design, catalytic performance and synergistic effects. *Chem. Eng. J.* **2023**, *477*, 146961. [CrossRef]
18. Tian, R.; Dong, H.; Chen, J.; Li, R.; Xie, Q. Amorphous Co_3O_4 nanoparticles-decorated biochar as an efficient activator of peroxymonosulfate for the removal of sulfamethazine in aqueous solution. *Sep. Purif. Technol.* **2020**, *250*, 117246. [CrossRef]
19. Ji, X.; Huang, J.-W.; Liu, W.-J.; Yu, H.-Q. Pyrolysis of biomass wastes to N-doped biochar-stabilized Co nanoparticles for efficient pollutant degradation via peroxymonosulfate activation. *ACS ES&T Eng.* **2021**, *1*, 1715–1724.
20. Pei, W.; Wang, Y.; Liu, Y.; Zhou, L.; Lei, J.; Zhang, J. Activation of peroxymonosulfate by $LaCO_3OH$ coupled with N, S Co-doped graphene for levofloxacin degradation. *Sep. Purif. Technol.* **2024**, *344*, 127157. [CrossRef]
21. Zhao, J.; Li, H.; Wang, Y.; Yu, J.; Li, N.; Wang, S. Cu/CuO-decorated peanut-shell-derived biochar for the efficient degradation of tetracycline via peroxymonosulfate activation. *Catalysts* **2023**, *13*, 1246. [CrossRef]
22. Lu, H.; Xu, G.; Gan, L. N doped activated biochar from pyrolyzing wood powder for prompt BPA removal via peroxymonosulfate activation. *Catalysts* **2022**, *12*, 1449. [CrossRef]
23. Song, N.; Wang, Y.; Li, Y.; Liu, Y.; Wang, Q.; Wang, T. The activation mechanism of peroxymonosulfate and peroxydisulfate by modified hydrochar: Based on the multiple active sites formed by N and Fe. *Environ. Pollut.* **2024**, *341*, 122981. [CrossRef] [PubMed]
24. Supraja, K.V.; Doddapaneni, T.R.K.C.; Ramasamy, P.K.; Kaushal, P.; Ahammad, S.Z.; Pollmann, K.; Jain, R. Critical review on production, characterization and applications of microalgal hydrochar: Insights on circular bioeconomy through hydrothermal carbonization. *Chem. Eng. J.* **2023**, *473*, 145059. [CrossRef]
25. Sun, Y.; Liu, C.; Zan, Y.; Miao, G.; Wang, H.; Kong, L. Hydrothermal carbonization of microalgae (*Chlorococcum* sp.) for porous carbons with high Cr(VI) adsorption performance. *Appl. Biochem. Biotech.* **2018**, *186*, 414–424. [CrossRef]
26. Jalilian, M.; Bissessur, R.; Ahmed, M.; Hsiao, A.; He, Q.S.; Hu, Y. A review: Hydrochar as potential adsorbents for wastewater treatment and CO_2 adsorption. *Sci. Total Environ.* **2024**, *914*, 169823. [CrossRef]
27. Funke, A.; Ziegler, F. Hydrothermal carbonization of biomass: A summary and discussion of chemical mechanisms for process engineering. *Biofuel. Bioprod. Biorefining* **2010**, *4*, 160–177. [CrossRef]
28. Wang, L.; Guo, Y.; Zhu, Y.; Li, Y.; Qu, Y.; Rong, C.; Ma, X.; Wang, Z. A new route for preparation of hydrochars from rice husk. *Bioresour. Technol.* **2010**, *101*, 9807–9810. [CrossRef] [PubMed]
29. Wang, G.; Nie, X.; Ji, X.; Quan, X.; Chen, S.; Wang, H.; Yu, H.; Guo, X. Enhanced heterogeneous activation of peroxymonosulfate by Co and N codoped porous carbon for degradation of organic pollutants: The synergism between Co and N. *Environ. Sci-Nano* **2019**, *6*, 399–410. [CrossRef]
30. Yang, L.; Wei, Z.; Guo, Z.; Chen, M.; Yan, J.; Qian, L.; Han, L.; Li, J.; Gu, M. Significant roles of surface functional groups and Fe/Co redox reactions on peroxymonosulfate activation by hydrochar-supported cobalt ferrite for simultaneous degradation of monochlorobenzene and p-chloroaniline. *J. Hazard. Mater.* **2023**, *445*, 130588. [CrossRef]
31. Wang, L.; Yin, G.; Chang, Y.; Qiao, S. Carbon-rich and low-ash hydrochar formation from sewage sludge by alkali-thermal hydrolysis coupled with acid-assisted hydrothermal carbonization. *Waste Manag.* **2024**, *177*, 182–195. [CrossRef] [PubMed]
32. Wu, F.; Zhang, R.; Zhou, J. Shrimp-shell-derived carbon dots for quantitative detection by fluorometry and colorimetry: A new analytic chemistry experiment for university education. *J. Chem. Educ.* **2024**, *101*, 2784–2789. [CrossRef]
33. Hu, G.; Ge, L.; Li, Y.; Mukhtar, M.; Shen, B.; Yang, D.; Li, J. Carbon dots derived from flax straw for highly sensitive and selective detections of cobalt, chromium, and ascorbic acid. *J. Colloid. Interf. Sci.* **2020**, *579*, 96–108. [CrossRef]
34. Hu, C.; Chen, Q.; Wu, S.; Wang, J.; Zhang, S.; Chen, L. Coupling harmful algae derived nitrogen and sulfur co-doped carbon nanosheets with CeO_2 to enhance the photocatalytic degradation of isothiazolinone biocide. *J. Environ. Manag.* **2024**, *356*, 120621. [CrossRef]
35. Ke, J.; Xu, D.S.; Zhou, Y.; Zhang, X.Y.; Liu, J. Confined cobalt oxide embedded into hierarchical bismuth tungstate in S-scheme micro-heterojunction for enhanced air purification. *Sep. Purif. Technol.* **2022**, *299*, 121806. [CrossRef]
36. Wei, Y.; Liu, X.; Wang, Z.; Chi, Y.; Yue, T.; Dai, Y.; Zhao, J.; Xing, B. Adsorption and catalytic degradation of preservative parabens by graphene-family nanomaterials. *Sci. Total Environ.* **2022**, *806*, 150520. [CrossRef]
37. Guo, S.; Wang, H.J.; Yang, W.; Fida, H.; You, L.M.; Zhou, K. Scalable synthesis of Ca-doped alpha-Fe_2O_3 with abundant oxygen vacancies for enhanced degradation of organic pollutants through peroxymonosulfate activation. *Appl. Catal. B-Environ.* **2020**, *262*, 12. [CrossRef]

38. Antonopoulou, M.; Liles, A.; Spyrou, A.; Vlastos, D.; Koronaiou, L.-A.; Lambropoulou, D. Assessment of UV-C/peroxymonosulfate process for the degradation of parabens mixture: Efficiency under different conditions, transformation pathways and ecotoxicity evolution. *J. Environ. Chem. Eng.* **2024**, *12*, 112044. [CrossRef]
39. Zhu, Z.; Yan, J.; Wang, M.; Zhu, H.; Li, X.; Wu, L. Insights into hydrangea-like $NiCo_2S_4$ activating peroxymonosulfate for efficient degradation of atrazine. *Chem. Eng. J.* **2023**, *477*, 146876. [CrossRef]
40. Liang, C.; Su, H.-W. Identification of sulfate and hydroxyl radicals in thermally activated persulfate. *Ind. Eng. Chem. Res.* **2009**, *48*, 5558–5562. [CrossRef]
41. Xu, T.; Chen, J.; Chen, X.; Xie, H.; Wang, Z.; Xia, D.; Tang, W.; Xie, H. Prediction models on *pK*a and base-catalyzed hydrolysis kinetics of parabens: Experimental and quantum chemical studies. *Environ. Sci. Technol.* **2021**, *55*, 10. [CrossRef]
42. Li, Y.; Zhang, S.; Qin, Y.; Yao, C.; An, Q.; Xiao, Z.; Zhai, S. Preparation of cobalt/hydrochar using the intrinsic features of rice hulls for dynamic carbamazepine degradation via efficient PMS activation. *J. Environ. Chem. Eng.* **2022**, *10*, 108659. [CrossRef]
43. Zhou, C.Y.; Liang, Y.T.; Xia, W.; Almatrafi, E.; Song, B.A.; Wang, Z.; Zeng, Y.; Yang, Y.; Shang, Y.; Wang, C.; et al. Single atom Mn anchored on N-doped porous carbon derived from *spirulina* for catalyzed peroxymonosulfate to degradation of emerging organic pollutants. *J. Hazard. Mater.* **2023**, *441*, 129871. [CrossRef] [PubMed]